

















**Einstein Probe discovery of EP J005245.1–722843:  
a rare BeWD binary in the Small Magellanic Cloud?**

A. MARINO <sup>1,2</sup> H. N. YANG <sup>3,4,5</sup> F. COTI ZELATI <sup>1,2</sup> N. REA <sup>1,2</sup> S. GUILLOT <sup>6</sup> G. K. JAISAWAL <sup>7</sup>  
C. MAITRA <sup>4</sup> J.-U. NESS <sup>8</sup> F. HABERL <sup>4</sup> E. KUULKERS <sup>9</sup> W. YUAN,<sup>3,5</sup> H. FENG,<sup>10</sup> L. TAO,<sup>10</sup> C. JIN,<sup>3,5</sup>  
H. SUN <sup>3</sup> W. ZHANG,<sup>3</sup> W. CHEN,<sup>3,5</sup> E. P. J. VAN DEN HEUVEL,<sup>11</sup> R. SORIA <sup>12,13,14</sup> B. ZHANG <sup>15,16</sup> S.-S. WENG,<sup>17</sup>  
L. JI,<sup>18</sup> G. B. ZHANG,<sup>19</sup> X. PAN,<sup>3</sup> Z. LV,<sup>3,5</sup> C. ZHANG,<sup>3,5</sup> Z. X. LING,<sup>3,5</sup> Y. CHEN,<sup>10</sup> S. JIA,<sup>10,5</sup> Y. LIU,<sup>3</sup> H. Q. CHENG,<sup>3</sup>  
D. Y. LI,<sup>3</sup> K. GENDREAU <sup>20</sup> M. NG <sup>21</sup> AND T. STROHMAYER <sup>20,22</sup>

<sup>1</sup>*Institute of Space Sciences (ICE, CSIC), Campus UAB, Carrer de Can Magrans s/n, 08193, Barcelona, Spain*

<sup>2</sup>*Institut d'Estudis Espacials de Catalunya (IEEC), Esteve Terradas 1, RDIT Building, Of. 212 Mediterranean Technology Park (PMT), 08860, Castelldefels, Spain*

<sup>3</sup>*National Astronomical Observatories, Chinese Academy of Sciences, Beijing, 100101, People's Republic of China*

<sup>4</sup>*Max-Planck-Institut für extraterrestrische Physik, Gießenbachstraße 1, D-85748 Garching bei München, Germany*

<sup>5</sup>*School of Astronomy and Space Sciences, University of Chinese Academy of Sciences, Beijing, 100049, People's Republic of China*

<sup>6</sup>*IRAP, CNRS, 9 avenue du Colonel Roche, BP 44346, 31028 Toulouse Cedex 4, France*

<sup>7</sup>*DTU Space, Technical University of Denmark, Elektrovej 327-328, DK-2800 Lyngby, Denmark*

<sup>8</sup>*European Space Agency (ESA), European Space Astronomy Centre (ESAC), Camino Bajo del Castillo s/n, E-28692 Villanueva de la Cañada, Madrid, Spain*

<sup>9</sup>*European Space Agency (ESA), European Space Research and Technology Centre (ESTEC), Keplerlaan 1, 2201 AZ Noordwijk, The Netherlands*

<sup>10</sup>*Key Laboratory of Particle Astrophysics, Institute of High Energy Physics, Chinese Academy of Sciences, Beijing 100049, People's Republic of China*

<sup>11</sup>*Anton Pannekoek Institute for Astronomy, University of Amsterdam, PO Box 94249, 1090 GE Amsterdam, The Netherlands*

<sup>12</sup>*INAF – Osservatorio Astrofisico di Torino, Strada Osservatorio 20, I-10025 Pino Torinese, Italy*

<sup>13</sup>*Sydney Institute for Astronomy, School of Physics A28, The University of Sydney, Sydney, NSW 2006, Australia*

<sup>14</sup>*College of Astronomy and Space Sciences, University of the Chinese Academy of Sciences, Beijing 100049, People's Republic of China*

<sup>15</sup>*Nevada Center for Astrophysics, University of Nevada Las Vegas, NV 89154, USA*

<sup>16</sup>*Department of Physics and Astronomy, University of Nevada Las Vegas, NV 89154, USA*

<sup>17</sup>*Department of Physics and Institute of Theoretical Physics, Nanjing Normal University, Nanjing, People's Republic of China*

<sup>18</sup>*School of Physics and Astronomy, Sun Yat-sen University, Zhuhai, 519082, People's Republic of China*

<sup>19</sup>*Yunnan Observatories, Chinese Academy of Sciences, Kunming 650216, People's Republic of China*

<sup>20</sup>*Astrophysics Science Division, NASA's Goddard Space Flight Center, Greenbelt, MD 20771, USA*

<sup>21</sup>*MIT Kavli Institute for Astrophysics and Space Research, Massachusetts Institute of Technology, Cambridge, MA 02139, USA*

<sup>22</sup>*Joint Space-Science Institute, NASA Goddard Space Flight Center, Greenbelt, MD 20771, USA*

(Received July, 2024)

Submitted to ApJL

ABSTRACT

On May 27 2024, the Wide-field X-ray Telescope onboard the *Einstein Probe* (EP) mission detected enhanced X-ray emission from a new transient source in the Small Magellanic Cloud (SMC) during its commissioning phase. Prompt follow-up with the EP Follow-up X-ray Telescope, the *Swift* X-ray Telescope and *NICER* have revealed a very soft, thermally emitting source (kT~0.1 keV at the outburst peak) with an X-ray luminosity of  $L \sim 4 \times 10^{38}$  erg s<sup>-1</sup>, labelled EP J005245.1–722843. This super-soft outburst faded very quickly in a week time. Several emission lines and absorption edges were present in the X-ray spectrum, including deep Nitrogen (0.67 keV) and Oxygen (0.87 keV) absorption edges. The X-ray emission resembles the SSS phase of typical nova outbursts from an accreting white dwarf (WD)

in a binary system, despite the X-ray source being historically associated with an O9-B0e massive star exhibiting a 17.55 days periodicity in the optical band. The discovery of this super-soft outburst suggests that EP J005245.1–722843 is a BeWD X-ray binary: an elusive evolutionary stage where two main-sequence massive stars have undergone a common envelope phase and experienced at least two episodes of mass transfer. In addition, the very short duration of the outburst and the presence of Ne features hint at a rather massive, i.e., close to the Chandrasekhar limit, Ne-O WD in the system.

*Keywords:* accretion, accretion disks – binaries: close – Magellanic Clouds – stars: individual: (EP J0052.9–7230) – white dwarfs

## 1. INTRODUCTION

Be-white dwarf X-ray binary systems (BeWDs) are a subclass of X-ray binaries where a white dwarf (WD) accretes matter from a Be-type main-sequence star. Binary evolution models predict that BeWDs should be about seven times more common than Be-neutron star (BeNS) systems (Raguzova 2001). Population synthesis models (Zhu et al. 2023) indicate that BeWDs originate from binaries initially composed of a Be star and a subdwarf O or B star. A substantial fraction of these systems can evolve either into red giants (via merging of the WD with a non-degenerated star; 60–70% of the cases), or into double WDs detectable by the LISA mission as sources of gravitational wave emission (30–40%). However, BeWDs have been so far relatively elusive. On the one hand,  $\gamma$  Cas analogs, a class of Be stars showing an excess in hard X-rays, are largely considered to be BeWD binaries, although the matter is still controversial (see, e.g. Gies et al. 2023, and references therein). On the other hand, a few confirmed Be binaries which show instead rather soft X-ray outbursts, have also been identified as BeWD (Kahabka et al. 2006; Sturm et al. 2012; Coe et al. 2020; Haberl et al. 2020; Kennea et al. 2021). The emission from the latter sources in outburst is typically characterized by very soft X-ray spectra with no detectable X-ray emission above  $>2$  keV, indicative of nuclear burning on the WD surface. In this regime, BeWDs can be classified as Super-Soft Sources (SSS) (Cracco et al. 2018), a group of sources that includes various types of X-ray systems powered by thermonuclear burning onto the surface of an accreting WD (Greiner et al. 1991). This category also encompasses novae during their SSS phase (e.g. Chomiuk et al. 2021). The lack of sensitive wide-field soft X-ray monitors has made the detection of outbursts from BeWDs rather challenging, especially during the rising phase. On May 27th 2024, the Wide-field X-ray Telescope (WXT) onboard the *Einstein Probe* (EP) mission detected enhanced X-ray emission from a new transient source, EP J005245.1–722843 (J0052 hereafter), in the SMC during its commissioning phase (Yang et al. 2024). This source was promptly iden-

tified as CXOU J005245.0–722844, following a serendipitous 52-s observation of the field by the *Neil Gehrels Swift Observatory* (*Swift*) X-ray Telescope (XRT) a few hours later (Kennea et al. 2024; Gaudin et al. 2024), as part of the *Swift* Small Magellanic Cloud Survey (SCUBED; Kennea et al. 2018). Two follow-up NICER observations on May 28th and 29th revealed a rapid decrease in the X-ray count rate between the two observations (Jaisawal et al. 2024). The source has a bright optical counterpart (average magnitude of  $G \sim 14.9$ ), which has been first classified as an O9-B0e star by (Antoniou et al. 2009) and later suggested to belong to the B0 class based also on its spectrum (Sheets et al. 2013; Maravelias et al. 2014; Gaudin et al. 2024). The companion star has an estimated age of  $\sim 40$  Myears, according to the age of the OB population in that region of the SMC (Antoniou et al. 2019). The long-term optical light curve shows a periodicity at  $\sim 17.55$  days, which is likely related to the orbital period of the system (Sarraj et al. 2012; Treiber et al. 2024). This Letter reports on the classification of this source as a BeWD following the discovery of its super-soft outburst by EP and its X-ray evolution. In the following, we adopt the position listed in the *Chandra* Source Catalog Release 2.1 (Evans et al. 2010), R.A. =  $00^{\text{h}}52^{\text{m}}45^{\text{s}}.13$ , decl. =  $-72^{\circ}28'43''.87$  (J2000.0) and a distance of 62 kpc (Graczyk et al. 2020). All parameter uncertainties are quoted at a  $1\sigma$  confidence level unless otherwise stated.

## 2. OBSERVATIONS AND DATA REDUCTION

In this paper, we have used observations from various X-ray telescopes, including the WXT and Follow-up X-ray Telescope (FXT) onboard EP, *Swift*, *NICER* and *XMM-Newton*, as well as archival *Chandra* observations (see Table 1 for details).

### 2.1. Einstein Probe

As a space observatory to discover and characterize X-ray transients, EP (Yuan et al. 2022) carries two instruments, the WXT and FXT. EP was launched on January 9, 2024 into a low-Earth circular orbit of 592 km

**Table 1.** Journal of the 2024 X-ray observations of J0052 presented in this work.

Telescope/Instrument (setup)	Obs ID	Start – End time (UTC)	Exposure (ks)	Epochs <sup>†</sup>
		Mmm DD hh:mm:ss		
EP/WXT	13600006246	May 25 11:06:46 – May 27 06:28:12	67.9	
EP/WXT	13600006247	May 27 08:02:48 – May 27 09:39:06	2.0	
EP/WXT	13600006248	May 27 09:39:06 – May 29 03:22:17	63.0	
<i>Swift</i> /XRT (PC)	03111173076	May 27 22:29:57 – May 27 22:30:50	0.052	
EP/WXT	08500000102	May 28 04:51:10 – May 28 06:26:53	1.6	
EP/FXT (PW)	08500000102	May 28 05:31:05 – May 28 06:23:21	1.5	1
<i>Swift</i> /XRT (WT)	00033745002	May 28 15:40:13 – May 28 17:19:37	1.9	2
<i>NICER</i> /XTI	7204550101	May 28 16:56:06 – May 28 23:24:20	4.1	3,4,5,6
<i>NICER</i> /XTI	7204550102	May 29 11:26:10 – May 30 00:00:00	6.0	7,8,9,10,11,12
<i>NICER</i> /XTI	7204550103	May 30 01:21:10 – May 30 23:22:00	8.0	13,14,15,16
<i>NICER</i> /XTI	7204550104	May 31 00:33:30 – May 31 21:01:21	6.4	17,18
<i>NICER</i> /XTI	7204550105	Jun 1 04:32:49 – Jun 1 17:16:20	1.9	19
<i>NICER</i> /XTI	7204550106	Jun 2 05:09:40 – Jun 2 17:59:00	5.8	20
<i>NICER</i> /XTI	7204550107	Jun 2 23:46:40 – Jun 3 23:09:40	3.4	21
<i>NICER</i> /XTI	7204550108	Jun 4 00:50:20 – Jun 4 23:59:20	1.9	
EP/FXT (FF)	08500000107	Jun 4 12:15:38 – Jun 4 16:19:28	9.1	
<i>NICER</i> /XTI	7204550109	Jun 5 10:33:20 – Jun 5 13:49:20	1.3	
<i>NICER</i> /XTI	7204550110	Jun 6 02:24:40 – Jun 6 22:23:00	0.8	
<i>NICER</i> /XTI	7204550111	Jun 6 23:43:40 – Jun 7 21:49:40	8.5	
<i>NICER</i> /XTI	7204550112	Jun 8 10:14:20 – Jun 8 18:03:00	0.3	
<i>Swift</i> /XRT (PC)	00033745004	Jun 13 20:35:38 – Jun 13 22:32:52	2.5	
<i>XMM-Newton</i> /EPIC-pn (SW)	0935191301	Jun 14 19:12:05 – Jun 15 03:59:07	31.6	
<i>XMM-Newton</i> /EPIC-MOS1 (T)	0935191301	Jun 14 19:26:34 – Jun 15 03:54:49	27.4	
<i>XMM-Newton</i> /EPIC-MOS2 (T)	0935191301	Jun 14 19:26:51 – Jun 15 03:54:39	29.4	
<i>Swift</i> /XRT (PC)	00033745005	Jun 15 02:31:09 – Jun 15 21:52:53	1.6	
<i>Swift</i> /XRT (PC)	00033745006	Jun 17 19:09:39 – Jun 17 21:12:52	2.6	
<i>Swift</i> /XRT (PC)	00033745007	Jun 19 18:35:06 – Jun 19 18:56:53	1.3	

**Notes.** FF: full frame; PW: Partial Window; PC: Photon Counting; WT: Windowed Timing; SW: Small Window; T: Timing; <sup>†</sup>: the observations considered for the spectral analysis in this paper.

height with an orbital period of 97 minutes. The WXT employs Lobster-eye micro-pore optics (MPO) to provide an instantaneous field-of-view of  $\sim 3600$  square degrees. The instrument comprises 12 modules, each covering about 300 square degrees. Each module includes a mirror assembly with 36 MPO optics, an optical baffle, and a focal-plane detector array of CMOS sensors. The in-orbit calibrations of WXT have been completed, whose results are in excellent agreement with those of the on-ground calibrations (Cheng H., in preparation). J0052 was simultaneously detected by the CMOS detectors 14 and 37 of the WXT during observations on 2024 May 27 from 08:41:28 to 12:47:16 UTC. Data were processed using the `wxtpipeline` tool version 0.1.0. The source region was determined as a circle with a radius of 67 pixels (1 pixel  $\sim 0.136'$ ) centered on the source. In the field of view of WXT, there are multiple bright objects together with their cross-arms. Therefore, we carefully

selected a circle of radius 268 pixels nearby as the background region to minimize the influence of other bright objects.

The FXT was configured in partial window mode and full frame mode for the observations performed on May 28 and June 4, respectively. Data were processed using the `fxtchain` tool available within the FXT Data Analysis Software (FXTDAS). Source and background photons were extracted using a circle of radius  $70''$  centered on the source and a closeby circle of radius  $128''$ , respectively.

## 2.2. Swift

The XRT observations were processed using `xrtpipeline`, employing the latest version of CALDB (v. 20240522). We extracted photons using a  $20''$  circular region centered on the source. In the first observation (WT mode), we estimated the background with a

similar-sized region far from the source. In the second observation (PC mode), we used an annular region with inner and outer radii of  $45''$  and  $150''$  for background estimation. We then extracted light curves and spectra through the `xrtproducts` pipeline. For the last four observations, we combined the data (totaling 8 ks of exposure) and set a  $3\sigma$  upper limit on the net count rate of  $0.002 \text{ counts s}^{-1}$  (calculated over the 0.3–10 keV energy range using the `sosta` command). In the first two *Swift* observations considered in this work, the UVOT was operated in image mode, using the UVW1 filter in the first one and cycling through all available filters in the second one. In the last four observations, the UVOT was operated in event mode using the UVM2 filter. We used a circle with a radius of  $5''$  for the source and a nearby circle with a radius of  $10''$  devoid of optical sources for the background. For image mode data, we performed aperture photometry (properly corrected to infinite aperture) with `uvotsource`. The optical brightness in the UVM2 filter varied from  $\sim 12.6$  to  $13.2$  mag (Vega) between May 27 and June 19, without showing any clear monotonic trend. For event mode data, we processed the files with `coordinator` and `uvotscreen` and searched for periodic signals using the unbinned event files (see Sect. 3.4).

### 2.3. NICER

*NICER* data were processed using the `nicer12` pipeline with default screening settings (following the same prescriptions as in, e.g. [Marino et al. 2023](#)). Several *NICER* light curves showed irregular count rate increases during the outburst. To minimize charged particle contamination, we reprocessed the data with `nicer12`, setting `overonly_range` to 0–5 and `COR_RANGE` to  $> 1.5 \text{ GeV}/c$ . Any observation segment still affected by non X-ray flares after this procedure was neglected from the following analysis. The `nicer13-spect` pipeline was used to produce spectra and background files. In particular, the `scorpeon` model<sup>1</sup> with default settings was adopted for the creation of the background file.

### 2.4. XMM–Newton

The EPIC-pn onboard *XMM–Newton* was configured in the small window mode, while both EPIC-MOS cameras operated in timing mode. Data were processed using the Science Analysis System (SAS). We applied intensity filters to the time series of the entire field of view in the EPIC-pn data to remove several background flar-

ing episodes (which were also visible at low energies), resulting in a net on-source exposure time of  $\sim 15$  ks. No X-ray emission was detected at the source position. Using the `eupper` tool and assuming a circular region with a radius of 10 arcsec for the source photons along with an annulus with inner and outer radii of 10 and  $20''$  respectively for the background, we estimated a  $3\text{-}\sigma$  upper limit on the net count rate of  $0.007 \text{ counts s}^{-1}$  over the 0.3–10 keV energy range. Given the non-detection in the EPIC-pn data, we did not perform further analysis on the EPIC-MOS and RGS data.

### 2.5. Chandra

The field of J0052 was observed with the ACIS-I instrument on board the *Chandra* X-ray Observatory three times on July 20, 2002 (7.7 ks), April 25, 2006 (49.3 ks), and April 26, 2006 (47.4 ks). We processed the data using the CIAO software package. In 2002, J0052 was detected at a count rate of  $(1.9_{-0.8}^{+1.0}) \times 10^{-3} \text{ counts s}^{-1}$  (0.3–7 keV) at the 90% c.l., corresponding to a detection significance exceeding 99%. For the stacked observations from 2006, the count rate was  $(1.3_{-0.7}^{+0.6}) \times 10^{-4} \text{ counts s}^{-1}$  (0.3–7 keV), representing a  $\sim 3\sigma$  detection.

## 3. DATA ANALYSIS AND RESULTS

### 3.1. The EP/WXT light curve

The WXT light curve is shown in Figure 1. After removing spurious drops in count rates caused by instrumental artifacts, the analysis of the observations before and after the source detection revealed a rapid increase in emission starting around MJD 60456.8, with a linear rise at  $\sim 0.3 \text{ counts s}^{-1} \text{ day}^{-1}$ , peaking around MJD 60457.5 after approximately 0.6 days. This was followed by a slow linear decay at  $\sim 0.02 \text{ counts s}^{-1} \text{ day}^{-1}$  until around MJD 60458.8, and then a faster decay at  $\sim 0.23 \text{ counts s}^{-1} \text{ day}^{-1}$ .

### 3.2. X-ray spectral analysis

The X-ray flux and spectral shape of J0052 varied significantly over hours. Therefore, we extracted time-resolved spectra over intervals with approximately constant count rates. For *NICER* observations 7204550101, 7204550102, 7204550103, and 7204550104, we divided them into 4, 6, 4, and 2 epochs, respectively, extracting one spectrum for each. The signal was largely or completely background-dominated in all *NICER*, EP/FXT and *Swift*/XRT observations performed after June 2, so we excluded these spectra from further analysis. The final spectral sample consists therefore of 1 FXT, 1 XRT and 19 *NICER* time-resolved spectra, hereafter referred to as epochs (see Table 1 for a summary). We grouped

<sup>1</sup> [https://heasarc.gsfc.nasa.gov/docs/nicer/analysis\\_threads/scorpeon-overview/](https://heasarc.gsfc.nasa.gov/docs/nicer/analysis_threads/scorpeon-overview/)

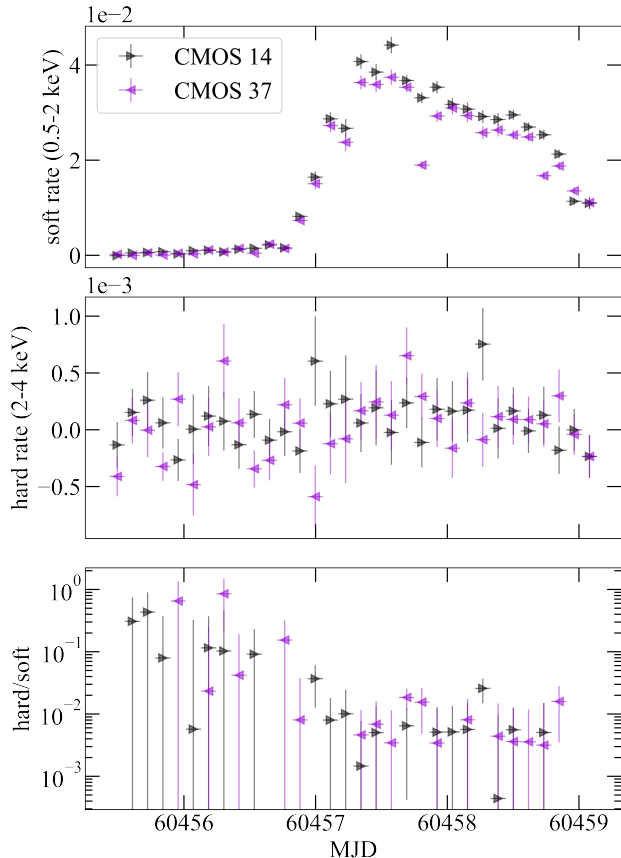


**Figure 1.** EP/WXT light curves of J0052 around the epoch of the outburst detection in the soft (0.5–2 keV; top) and hard (2–4 keV; middle) energy bands. The drop in the middle of the light curve of CMOS 37 is caused by instrumental effects. The time evolution of the hardness ratio is also plotted (bottom).

all the spectra ensuring a minimum of 25 counts per bin, allowing the use of the  $\chi^2$ -statistics. Figure 2 (a) shows the evolution of the extracted spectra of the source. We included data only where the source emission was above the background, which varied from spectrum to spectrum but was always within the 0.3–1.3 keV range. We note that despite the not-optimal calibration of *NICER* data below  $\sim 0.4$  keV<sup>2</sup>, we decided to retain data between 0.3 and 0.4 keV due to the source bright soft emission.

We performed the spectral analysis with *xspec* v.12.14.b (Arnaud 1996). A systematic error of 1% was included, as recommended by the *NICER* team<sup>3</sup>. The interstellar absorption was modelled through the *TBabs* component, with abundances from Wilms et al. (2000)

<sup>2</sup> [https://heasarc.gsfc.nasa.gov/docs/nicer/analysis\\_threads/cal-recommend/](https://heasarc.gsfc.nasa.gov/docs/nicer/analysis_threads/cal-recommend/)

<sup>3</sup> [https://heasarc.gsfc.nasa.gov/docs/nicer/analysis\\_threads/spectrum-systematic-error/](https://heasarc.gsfc.nasa.gov/docs/nicer/analysis_threads/spectrum-systematic-error/)

and cross sections from Verner et al. (1996). We derived the unabsorbed bolometric fluxes between 0.001 and 10 keV using the *cflux* convolution model. We initially adopted a simple absorbed blackbody model (*BBodyrad*) to fit the spectra. Although it matched the continuum reasonably well, the overall fit was poor, with significant unmodeled residuals (see, e.g., Figure 2, panel c). For *NICER*, artifacts like fluorescence lines from Earth’s atmosphere can result from improper background modeling. To check for these residuals, we re-extracted the spectrum from the brightest *NICER* snapshot using the *nicer13-spec* pipeline with the *bkgformat* option set to “script” instead of “file”, allowing a proper background fit with the continuum. The residuals in the best-fit model were identical regardless of the method used, indicating that the observed spectral features are real and not due to the background. These residuals include two edges, at 0.32 keV in *NICER* data, and at 0.47 keV in FXT data, likely due to calibration issues<sup>4</sup> and are not discussed. Instead, we detected intrinsic absorption edges from the source at energies of  $\sim 0.63$ ,  $\sim 0.88$  and  $\sim 1.0$  keV, although they almost never appeared all together in a single spectrum. Two localised excesses at about 0.5–0.7 keV and 0.9 keV were visible in Epochs 1–14 and 1, 3–6, respectively.

We tested four models to describe the spectra: (a) a *BBodyrad* component plus a set of absorption edges and Gaussians; (b) a *BBodyrad* component plus a set of absorption edges and an *APEC* model, which describes the emission spectrum from a collisionally-ionized diffuse gas; (c) a NLTE stellar atmosphere model, obtained employing the grid 003 of the *TMAP*<sup>5</sup> public repository (Rauch 2003) plus *APEC*; (d) a *SSS\_atm\_SMC* (Suleimanov et al. 2024)<sup>6</sup> plus *APEC*. In all fits including *APEC*, the abundance parameter was unconstrained, so that we consistently kept it fixed to 0.1, i.e., the SMC abundances. Models (a) and (b) describe the spectra equally well. Acceptable fits are obtained with model (c) only for spectra corresponding to the decay phase of the outburst, i.e., from Epoch 11 on. At the peak of the outburst, the model falls short in describing the emission above 0.8 keV. The maximum temperature allowed by the *TMAP* model might be indeed too low to account for the relatively hard spectra in Epochs 1–10. For similar

<sup>4</sup> See [https://heasarc.gsfc.nasa.gov/docs/nicer/analysis\\_threads/arf-rmf/](https://heasarc.gsfc.nasa.gov/docs/nicer/analysis_threads/arf-rmf/)

<sup>5</sup> Tübingen NLTE model-atmosphere package, [http://astro.uni-tuebingen.de/~rauch/TMAF/flux\\_HHeCNOeMgSiS\\_gen.html](http://astro.uni-tuebingen.de/~rauch/TMAF/flux_HHeCNOeMgSiS_gen.html)

<sup>6</sup> *SSS\_atm\_SMC* models the X-ray super-soft emission from a hot WD atmosphere with SMC abundances.

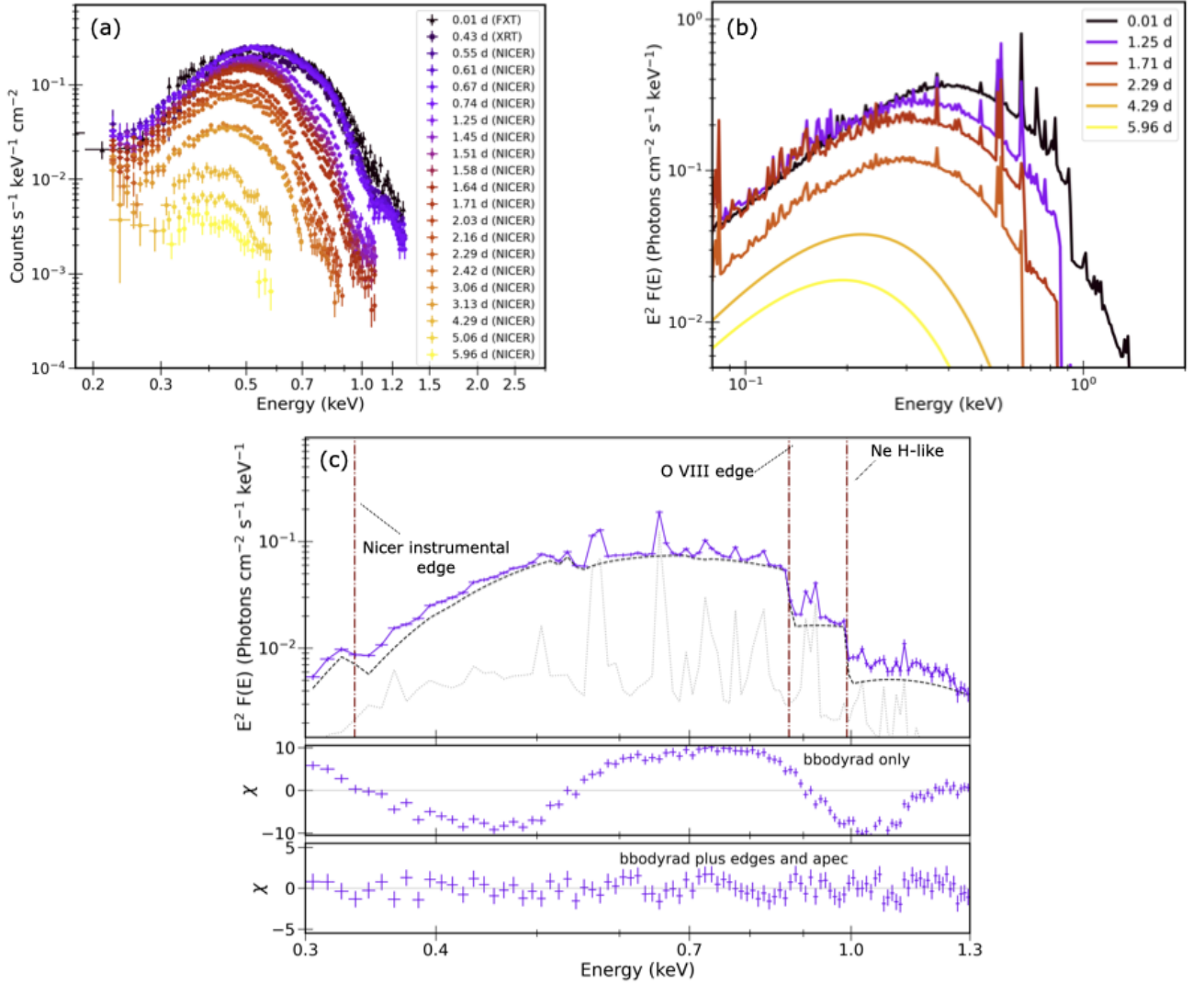


**Figure 2.** Summary plot for the spectral analysis performed for J0052. Panel (a): single spectra divided by each instrument’s effective area taken by EP/FXT (triangles), *Swift*/XRT (squares) and *NICER* (circles). The time for each spectrum is referenced from MJD 60458.23. Panel (b): best-fit unabsorbed models of selected observations. Panel (c): unfolded *NICER* spectrum taken during epoch 4 along with the best-fit model (top panel). The **bbodyrad** component is represented by a dashed black line, while the **apec** component is drawn with dotted silver line. The energies of the identified edges are marked with vertical maroon lines. The unmodelled and modelled residuals are shown in the middle and bottom panel.

reasons, model (d) is also inadequate to describe our data, especially at the peak. In the following, we will mainly consider the results obtained with model (b), being more physically motivated than model (a) and the only model able to describe coherently our entire data set.

We consistently obtained  $N_{\text{H}}$  values within the range of  $(1\text{--}2)\times 10^{21}\text{ cm}^{-2}$ . This range is significantly larger than the expected foreground value for the SMC, which is only  $\sim 6\times 10^{20}\text{ cm}^{-2}$  (Dickey & Lockman 1990). The discrepancy between our obtained and the expected  $N_{\text{H}}$  values might indicate the presence of local absorption along the line of sight, as has been suggested for other

SSS in the SMC (Coe et al. 2020; Kennea et al. 2021). From the blackbody normalization we estimated the radius of the blackbody emitting regions in each time-resolved spectrum, finding a range of about  $3\text{--}6\times 10^3\text{ km}$ . The best-fit values obtained for both the continuum and the edges are listed in Tables A1 and A2, respectively. The simultaneous evolution of the best-fit parameters can be observed in Figure 3.

### 3.3. Pre-outburst detections and post-outburst upper limits

The upper limit on the net count rate measured in the last four stacked *Swift*/XRT observations

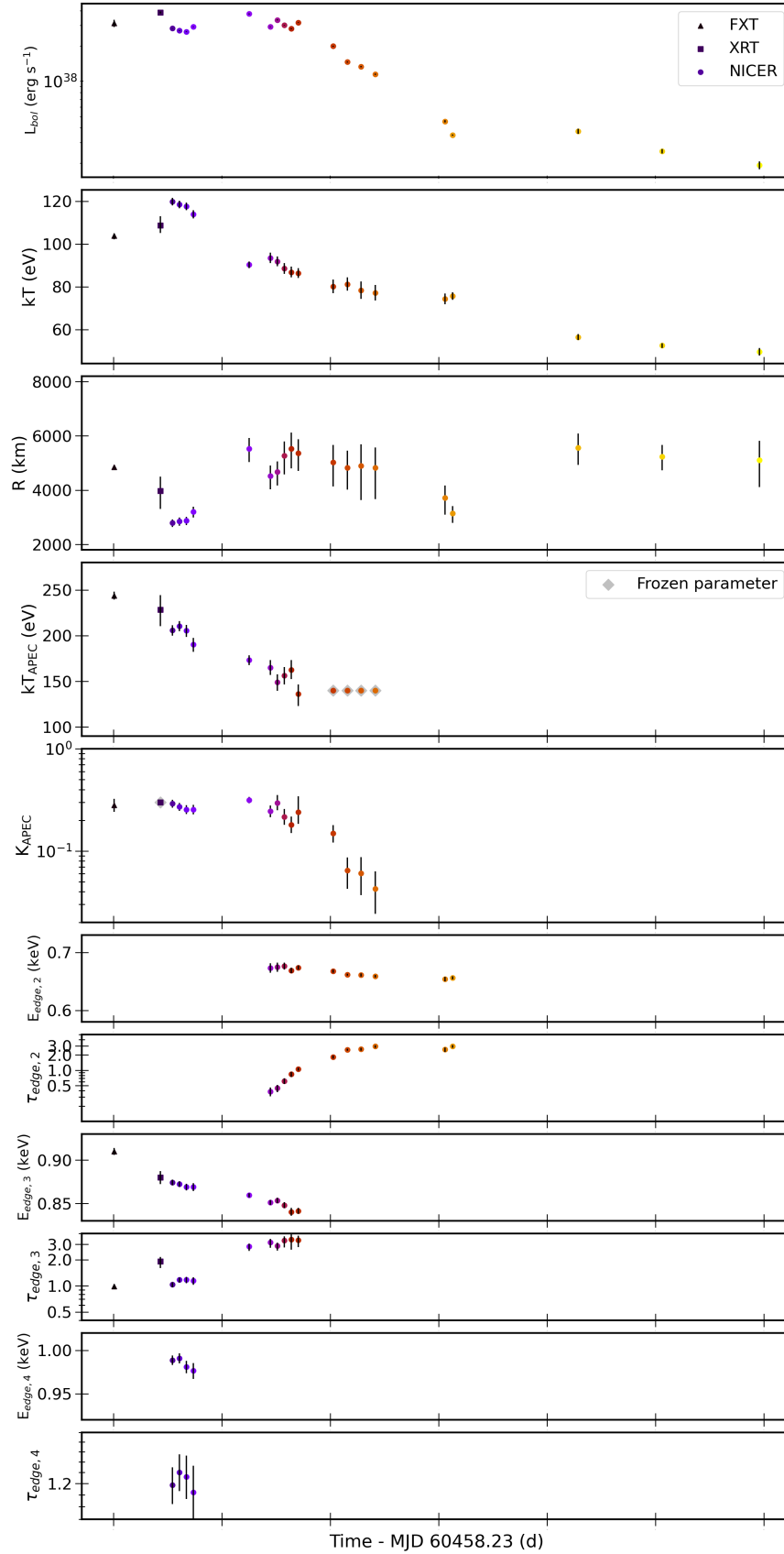


**Figure 3.** Best-fit spectral parameters obtained in this work and their evolution during the outburst. The color sequence is the same as the one used in Figure 2. See also Tables A1 and A2.

and in the *XMM-Newton*/EPIC-pn observation converts to unabsorbed bolometric fluxes of  $<6 \times 10^{-12}$  and  $<7 \times 10^{-13} \text{ erg cm}^{-2} \text{ s}^{-1}$ , respectively, assuming the same parameters measured in the latest *NICER* spectrum (see Table A1). On the other hand, the count rate recorded in the 2002 *Chandra* observation, which has a higher signal-to-noise ratio compared to the 2006 observations, corresponds to an observed flux of  $\approx 3 \times 10^{-14} \text{ erg cm}^{-2} \text{ s}^{-1}$  (0.3–8 keV; computed using the `srcflux` tool, assuming an absorbed power-law model with an absorption column density of  $2 \times 10^{21} \text{ cm}^{-2}$  and a photon index in the range of 0.5 to 1.5). This results in a luminosity of  $\approx 1.5 \times 10^{34} \text{ erg s}^{-1}$  (0.3–8 keV). For the 2006 observations, assuming the same spectral shape as above and scaling based on the count rate, we estimate a luminosity that is about an order of magnitude lower,  $\approx 10^{33} \text{ erg s}^{-1}$ .

### 3.4. Searches for periodic signals

To search for periodic signals, we used the data collected when the source was brightest and corrected the photon times of arrival to the barycenter of the Solar System. We considered data of the first two *NICER* observations and the first EP/FXT observation, all restricted to the 0.3–2 keV energy band to maximize the signal-to-noise ratio. *Swift*/UVOT data taken in event mode during the longest observation on June 17 were also searched. We then extracted power spectra from the unbinned event files from each dataset separately. No statistically significant signals were detected in any of the data. The  $3\sigma$  upper limits on the pulsed fraction were calculated (Israel & Stella 1996), resulting in:  $<4\%$  up to 2 kHz in the *NICER* data; between 10–16% up to 250 Hz in the EP/FXT data; between 7–10% up to 50 Hz in the *Swift*/UVOT data. For the *NICER* data, which had the highest signal-to-noise ratio, we also employed Fourier-domain acceleration search techniques using PRESTO<sup>7</sup> (Ransom et al. 2002) to search for signals up to 2 kHz. This analysis was conducted on the entire dataset of the first two observations as well as on 300-s data chunks. No statistically significant signal was detected. These results are consistent with those reported by Jaisawal et al. (2024).

## 4. DISCUSSION AND CONCLUSIONS

In this paper, we have presented the EP/WXT discovery of an X-ray outburst from the BeWD binary EP J005245.1–722843 (Antoniou et al. 2009) in the SMC and the follow-up X-ray observing campaign performed with EP/FXT, *NICER*, *Swift*/XRT, and *XMM-*

*Newton*/EPIC. The source experienced a rapid increase in bolometric luminosity from  $\sim 4 \times 10^{33} \text{ erg s}^{-1}$  before the onset of the outburst to  $\sim 4 \times 10^{38} \text{ erg s}^{-1}$  at the outburst peak. A slower decay over one order of magnitude in luminosity was then observed in about six days, after which the system was no longer detectable by *NICER*, likely due to being too faint, too soft, or both. An *XMM-Newton*/EPIC-pn observation set a stringent upper limit of  $<5 \times 10^{35} \text{ erg s}^{-1}$  on the bolometric luminosity of the source 12 days after the last *NICER* detection. This indicates a reduction in luminosity by at least three orders of magnitude during that period, marking the end of the outburst. We therefore conclude that the total duration of the outburst from J0052 ranged between 6 and 12 days, making it remarkably short. Throughout the entire outburst, the source consistently exhibited a soft spectral shape, with no emission detected beyond  $\sim 1.5 \text{ keV}$ . However, the observed spectrum was not as soft as typical SSS, whose emission usually cuts off at  $\sim 0.7 \text{ keV}$  (e.g. Orio et al. 2022), making this source somewhat peculiar. The spectra are well-modeled using a combination of a blackbody spectrum and an `apec` model. The source reached a blackbody temperature of  $\sim 120 \text{ eV}$  in about one day since the EP/WXT detection and then exhibited a rapid decay to  $\sim 50 \text{ eV}$  in less than a week. The blackbody radius showed an almost opposite trend, going from a minimum of  $\sim 2700 \text{ km}$  coincident with the  $kT$  peak to a maximum of  $\sim 6700 \text{ km}$  after about 2 days and then plateauing for the remainder of the outburst. Similar trends have been reported in the SSS phase of several novae, analysed as well with blackbody models (see, e.g., Page et al. 2015, 2020), although the peak temperatures were significantly lower than those seen in J0052. A more remarkable similarity in both the peak temperatures and the spectral shape, i.e., not soft enough for a canonical SSS, can be spotted in the outbursting BeWD binary MAXI J0158-744 (Li et al. 2012). The initial temporary decrease in the temperature observed between epochs 1 and 3 could also be due to variability in the early SSS phase as reported by Osborne et al. (2011) or could be an artefact due to intercalibration issues between FXT, XRT and *NICER*. We caution that blackbody models are only a crude approximation of the actual physics in SSS. Therefore, while the trends observed in the parameters are reliable, the specific values obtained for these parameters are less so. The attempt to model the thermal component with more physically reliable WD atmosphere models (Rauch 2003; Suleimanov et al. 2024) was instead not as successful. At the peak of the outburst, these models can not describe our data (as in MAXI J0158-744, Li et al. 2012), possibly because of the upper limit on the WD tem-

<sup>7</sup> <https://github.com/scottransom/presto>



perature being too stringent and/or some of the model assumptions being not applicable to this source. Good fits are instead obtained in the decline phase of the outburst, a stage where possibly the emission of our source resembles more that of a hot compact white dwarf.

Almost all the spectra analysed in this paper showed a dense and intricate array of discrete spectral features in absorption and emission. The  $\sim 0.63$  keV,  $\sim 0.87$  keV and  $\sim 0.98$  keV edges can be associated<sup>8</sup> with absorption edges from hydrogen-like species of N, O and Ne, respectively. Nitrogen, oxygen and neon features are often found in the X-ray spectra of novae and SSS (see, e.g. Ness et al. 2013; Drake et al. 2021; Bhargava et al. 2024) and they can be considered as a signature of a WD accretor. The additional emission lines are instead well-modelled by including in the fits a relatively cold, i.e.,  $kT_{\text{apec}} \sim 100 - 200$  eV, shocked gas emitting an APEC component. The presence of this component might suggest the presence of shocked ejecta around an emerging hot WD, as sometimes observed in novae with early turned-on SSS phases (see, e.g., Page et al. 2020). We conclude that the majority of the observed properties of the X-ray outburst of J0052, with the exception of the rather hard spectral shape at the outburst peak and its incompatibility with WD atmosphere models, are in line with the SSS phase of a nova eruption. In this scenario, the observed X-ray outburst would be explained by thermonuclear burning on the surface of the WD, and not by the initial thermonuclear runaway phase of a small-amplitude nova, as previously suggested by Gaudin et al. (2024) based only on the first *Swift* observation of the source. However, the duration of the observed super-soft outburst, i.e., about a week, stands out with respect to most novae in the SSS phase, which typically lasts tens to hundreds of days (e.g. Henze et al. 2010, but see Orio et al. 2023 for exceptions). The duration of an SSS phase depends primarily on the mass and chemical composition of the WD. WDs near the Chandrasekhar limit have shorter SSS phases since less accreted material is needed for a thermonuclear runaway. Conversely, higher hydrogen abundance in the accreted material slows the process (Hachisu et al. 2006). The combination of a  $\sim 10$  days duration, a peak effective temperature of  $\sim 120$  eV and a peak luminosity above  $10^{38}$  erg s<sup>-1</sup>, suggests the presence of a very massive object (Wolf et al. 2013; Soraisam et al. 2016). However, we caution that the existing literature may not be specifically tailored to the scenario of a WD accreting from a Be star. In addition, the presence of O and Ne features could be the signature of an

Ne-O WD in the system, which is among the most massive WDs, typically exceeding  $1.1 M_{\odot}$  (Taguchi et al. 2023). Future high-resolution optical and/or X-ray spectra might shed light on the chemical composition of the WD and potentially confirm the accreting star in J0052 as a Ne-O WD.

It is noteworthy that in novae, the SSS phase typically begins after an optical-to-UV brightening phase caused by the expanding WD photosphere, which usually lasts for weeks (e.g. Darnley et al. 2016). In the case of J0052, however, only a 0.5 magnitude increase in the optical band was observed six hours before the X-ray outburst (Gaudin et al. 2024), which would be unusual for a thermonuclear runaway-driven explosion. Similarly, a short-lived optical flare occurred just eleven hours before the X-ray outburst of the BeWD MAXI J0158-744 (Li et al. 2012). It is possible that the optical brightening in both that source and in J0052 might have occurred but went undetected due to the dominant emission from the optically bright Be companion star (as suggested by Li et al. 2012). Alternatively, an intrinsically short optical flare could be due the whole nova explosion being quick, possibly because of exceptionally low ejecta mass (Morii et al. 2013), as also suggested by Gaudin et al. (2024).

The ensemble of the X-ray spectral clues gathered in this work indicates that the compact object in J0052 is a massive, possibly Ne-O, WD. We therefore propose that J0052 is a BeWD binary. Such probably common but very elusive systems provide valuable insights into the evolution of binary stars, showcasing observable effects of the common envelope (CE) phase and mass transfer in massive star binaries. A binary system initially composed of two main-sequence stars of masses of about  $8M_{\odot}$  and  $6M_{\odot}$  with an orbital period of  $\sim 3$  days is a possible progenitor for J0052. Following conservative mass transfer as computed by Götberg et al. (2018), the system evolves into a  $2.1M_{\odot}$  He-star and a  $11.9M_{\odot}$  Be main-sequence star with an orbital period of about 21 days. According to the computations by Woosley (2019), such a He-star terminates its evolution as a Ne-O WD with a mass of  $1.23M_{\odot}$ , confirming results by Habets (1986b). During the evolution of the He-star, mass transfer to the Be star resumes, but the mass transfer is non-conservative, due to the He-star's convective envelope, which expands on a dynamical timescale, leading to the formation of a CE surrounding the Be star and the degenerate Ne-O core. When the envelope has expanded to the second Lagrangian point, it leads to the formation of a circumbinary disk with a mass of about  $0.9M_{\odot}$ . This causes the orbital period to decrease by a factor of about 0.8, resulting in a final orbital period of about 17 days (see section 4.3.8 of Tauris & van den Heuvel 2023 for

<sup>8</sup> We mostly refer to <https://xdb.lbl.gov/Section1/Sec.1-8.html> for the identification of these lines.

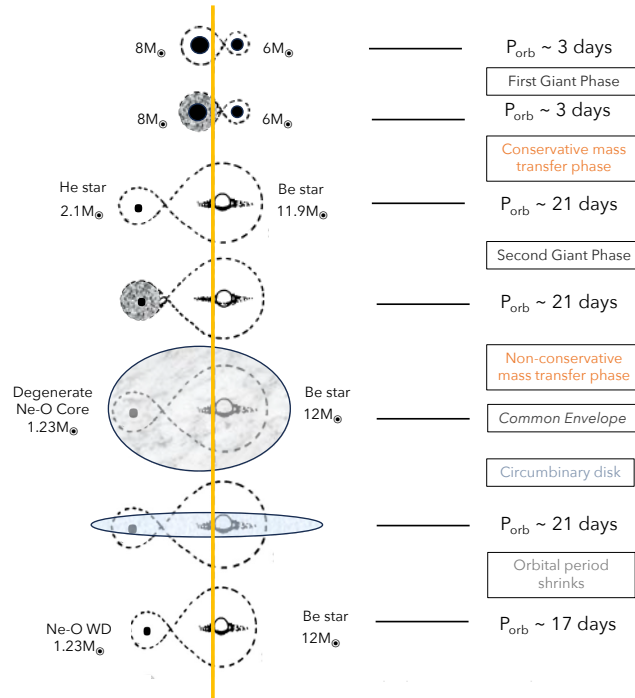


**Figure 4.** Schematic evolutionary path of J0052 as described in the text. This is the lower-mass analogue of the evolutionary model by [Habets \(1986a\)](#) for forming a Be- X-ray binary, here adapted for the case in which the accreting object is a massive Ne-O WD.

orbital period effects of a circumbinary disk). The disk will finally be expelled from the system. We sketch the proposed evolutionary scenario for J0052 in Figure 4. It is noteworthy that, despite the above scenario being only one of the possible models for the secular evolution of the binary system, the expected age of the system fits very well with the J0052 age, i.e., of about 40 Myears ([Antoniou et al. 2019](#)). Indeed, the initial  $8 M_{\odot}$  star takes approximately  $\sim 35$  Myears before evolving into a system with a Be star of about  $12\text{--}13 M_{\odot}$ , characterised by lifetimes of typically  $\sim 20$  Myears ([Schaller et al. 1992](#)). If the nature of the source is confirmed, this work may represent one of the very few cases where a X-ray outburst in such systems has been thoroughly monitored for most of its duration, from rise to decay. The unprecedented monitoring capabilities of *Einstein Probe* in the soft X-ray range are particularly well-suited to discovering super-soft outbursts from these sources, offering the opportunity to address many unresolved questions about them.

1 We thank the anonymous referee for their insightful  
 2 and useful comments. This work is based on data ob-  
 3 tained with *Einstein Probe*, a space mission supported  
 4 by Strategic Priority Program on Space Science of Chi-  
 5 nese Academy of Sciences, in collaboration with ESA,  
 6 MPE and CNES (Grant No. XDA15310000), the Strate-  
 7 gic Priority Research Program of the Chinese Academy  
 8 of Sciences (Grant No. XDB0550200), and the National  
 9 Key R&D Program of China (2022YFF0711500). This  
 10 work is also based on data obtained by: the Neil Gehrels  
 11 *Swift* Observatory (a NASA/UK/ASI mission) supplied  
 12 by the UK *Swift* Science Data Centre at the Univer-  
 13 sity of Leicester; *NICER*, a 0.2–12 keV X-ray telescope  
 14 operating on the International Space Station, funded  
 15 by NASA; *XMM-Newton*, an ESA science mission with  
 16 instruments and contributions directly funded by ESA  
 17 Member States and NASA. This paper employs a list  
 18 of Chandra datasets, obtained by the Chandra X-ray  
 19 Observatory, contained in the Chandra Data Collec-  
 20 tion (CDC) with doi:doi:10.25574/cdc.294. We thank  
 21 N. Schartel for approving Target of Opportunity ob-  
 22 servations with *XMM-Newton* in the Director’s Discre-  
 23 tionary Time and the *XMM-Newton* Science Operation  
 24 Center for scheduling and carrying out the observations.  
 25 Similarly, we thank the *Swift* team for approving and  
 26 performing our Target of Opportunity observations.

27 We acknowledge the support by the National Natu-  
 28 ral Science Foundation of China (Grant Nos. 12321003,  
 29 12103065, 12203071, 12333004, 12373040, 12021003),  
 30 the China Manned Space Project (Grant Nos. CMS-  
 31 CSST-2021-A13, CMS-CSST-2021-B11), and the Youth  
 32 Innovation Promotion Association of the Chinese  
 33 Academy of Sciences. We acknowledge the data re-

**Table A1.** Spectral analysis results using a black-body model for the continuum emission and `vapec`. The parameters that have been fixed are indicated in parenthesis. We consider MJD 60458.23 as reference time. Abundances in `vapec` fixed to 0.1.

Time (d)	nH ( $\times 10^{22}$ )	kT <sub>bb</sub> (eV)	R <sub>bb</sub> ( $\times 10^3$ km)	kT <sub>apec</sub> (eV)	N <sub>apec</sub>	L <sub>bol</sub> ( $\times 10^{38}$ erg/s)	$\chi^2$ (d.o.f.)
0.01	0.140 $^{+0.007}_{-0.006}$	100 $^{+1}_{-2}$	4.9 $\pm$ 0.1	240 $\pm$ 4	0.28 $\pm$ 0.04	3.1 $\pm$ 0.2	411(287)
0.43	0.180 $^{+0.016}_{-0.017}$	110 $^{+4}_{-3}$	4.0 $^{+0.7}_{-0.5}$	230 $^{+16}_{-18}$	(0.30)	3.90 $\pm$ 0.07	87(73)
0.55	0.140 $\pm$ 0.003	120 $\pm$ 2	2.8 $^{+0.2}_{-0.1}$	210 $\pm$ 6	0.29 $\pm$ 3	2.80 $\pm$ 0.02	98(90)
0.61	0.140 $^{+0.004}_{-0.003}$	120 $\pm$ 2	2.9 $^{+0.2}_{-0.1}$	210 $\pm$ 6	0.27 $^{+0.03}_{-0.02}$	2.70 $\pm$ 0.02	103(90)
0.67	0.140 $\pm$ 0.003	120 $\pm$ 2	2.9 $^{+0.2}_{-0.1}$	210 $^{+6}_{-7}$	0.25 $\pm$ 0.03	2.60 $\pm$ 0.02	107(90)
0.74	0.140 $\pm$ 0.004	110 $\pm$ 2	3.2 $\pm$ 0.2	190 $\pm$ 8	0.25 $\pm$ 0.03	2.90 $\pm$ 0.02	124(90)
1.25	0.170 $\pm$ 0.006	90 $\pm$ 2	5.5 $^{+0.5}_{-0.4}$	170 $\pm$ 5	0.30 $\pm$ 0.02	3.80 $\pm$ 0.03	100(79)
1.45	0.150 $^{+0.006}_{-0.005}$	94 $\pm$ 2	4.5 $^{+0.5}_{-0.4}$	170 $\pm$ 8	0.25 $\pm$ 0.03	2.90 $\pm$ 0.02	87(69)
1.51	0.150 $\pm$ 0.006	92 $\pm$ 2	4.7 $^{+0.5}_{-0.4}$	150 $\pm$ 5	0.30 $^{+0.06}_{-0.05}$	3.30 $\pm$ 0.03	84(65)
1.58	0.160 $^{+0.008}_{-0.007}$	89 $\pm$ 2	5.3 $^{+0.7}_{-0.5}$	160 $^{+9}_{-10}$	0.22 $\pm$ 0.04	3.00 $\pm$ 0.02	85(64)
1.64	0.160 $\pm$ 0.008	87 $^{+3}_{-2}$	5.5 $^{+0.7}_{-0.6}$	160 $^{+11}_{-10}$	0.18 $^{+0.04}_{-0.03}$	2.80 $\pm$ 0.02	79(63)
1.71	0.160 $^{+0.008}_{-0.007}$	86 $\pm$ 2	5.4 $^{+0.7}_{-0.5}$	140 $^{+10}_{-13}$	0.24 $^{+0.10}_{-0.06}$	3.20 $\pm$ 0.03	71(63)
2.03	0.140 $^{+0.007}_{-0.006}$	80 $\pm$ 3	5.0 $^{+0.9}_{-0.6}$	(140)	0.15 $\pm$ 0.03	2.00 $\pm$ 0.02	58(37)
2.16	0.140 $\pm$ 0.008	81 $\pm$ 3	4.8 $^{+0.8}_{-0.6}$	(140)	0.06 $\pm$ 0.02	1.50 $\pm$ 0.01	39(42)
2.29	0.140 $^{+0.011}_{-0.010}$	78 $\pm$ 4	4.9 $^{+1.3}_{-0.8}$	(140)	0.06 $^{+0.03}_{-0.02}$	1.34 $\pm$ 0.02	40(41)
2.42	0.140 $^{+0.011}_{-0.010}$	77 $\pm$ 4	4.8 $^{+1.2}_{-0.7}$	(140)	0.04 $\pm$ 0.02	1.20 $\pm$ 0.01	30(42)
3.06	0.130 $\pm$ 0.010	74 $^{+3}_{-2}$	3.7 $^{+0.6}_{-0.5}$	-	-	0.46 $\pm$ 0.01	32(40)
3.13	0.110 $\pm$ 0.010	76 $\pm$ 2	3.1 $\pm$ 0.3	-	-	0.35 $\pm$ 0.01	35(42)
4.29	(0.130)	56 $\pm$ 2	5.6 $^{+0.6}_{-0.5}$	-	-	0.38 $\pm$ 0.02	24(25)
5.06	(0.130)	53 $\pm$ 1	5.2 $^{+0.5}_{-0.4}$	-	-	0.25 $\pm$ 0.01	35(26)
5.96	(0.130)	50 $\pm$ 2	5.1 $^{+1.0}_{-0.7}$	-	-	0.19 $\pm$ 0.02	16(21)

*Facilities:* Einstein Probe, Swift, NICER, XMM–Newton, Chandra

*Software:* CIAO v4.16.0 (Fruscione et al. 2006), fxtsoftware v1.05, HEASOFT v6.33.2 (Nasa High Energy Astrophysics Science Archive Research Center (Heasarc) 2014), Matplotlib v3.9 (Hunter 2007), NICERDAS v12, SAS v21.0.0 (Gabriel et al. 2004), XSPEC v12.14.0h (Arnaud 1996)

## APPENDIX

## REFERENCES

- Antoniou, V., Hatzidimitriou, D., Zezas, A., & Reig, P. 2009, ApJ, 707, 1080
- Antoniou, V., Zezas, A., Drake, J. J., et al. 2019, ApJ, 887, 20
- Arnaud, K. A. 1996, in Astronomical Society of the Pacific Conference Series, Vol. 101, Astronomical Data Analysis Software and Systems V, ed. G. H. Jacoby & J. Barnes, 17
- Bhargava, Y., Dewangan, G. C., Anupama, G. C., et al. 2024, MNRAS, 528, 28
- Chomiuk, L., Metzger, B. D., & Shen, K. J. 2021, ARA&A, 59, 391
- Coe, M. J., Kennea, J. A., Evans, P. A., & Udalski, A. 2020, MNRAS, 497, L50
- Cracco, V., Orio, M., Ciroti, S., et al. 2018, ApJ, 862, 167

**Table A2.** Spectral analysis of the absorption edges included in the fits. The parameters that have been fixed are indicated in parenthesis. We consider MJD 60458.23 as reference time.

Absorption edges								
Time	$E_{e,1}$	$\tau_{e,1}$	$E_{e,2}$	$\tau_{e,2}$	$E_{e,3}$	$\tau_{e,3}$	$E_{e,4}$	$\tau_{e,4}$
(d)	(keV)	-	(keV)	-	(keV)	-	(keV)	-
0.01	0.370±0.006	(1.0)	-	-	0.910±0.004	1.0±0.6	-	-
0.43	-	-	-	-	0.870±0.001	3.0 <sup>+2.0</sup> <sub>-0.8</sub>	-	-
0.55	0.330±0.005	(1.0)	-	-	0.870±0.003	1.0±0.7	0.990 <sup>+0.006</sup> <sub>-0.005</sub>	1.20±0.08
0.61	0.330±0.005	(1.0)	-	-	0.870±0.003	1.2±0.1	0.990±0.006	1.20±0.08
0.67	0.330±0.005	(1.0)	-	-	0.870±0.004	1.2±0.1	0.980±0.007	1.20±0.10
0.74	0.340 <sup>+0.005</sup> <sub>-0.006</sub>	(1.0)	-	-	0.870±0.005	1.1±0.1	0.980±0.009	1.20±0.12
1.25	0.340 <sup>+0.005</sup> <sub>-0.006</sub>	(1.0)	-	-	0.870±0.002	2.8 <sup>+0.3</sup> <sub>-0.2</sub>	-	-
1.45	0.330±0.007	(1.0)	0.670±0.008	0.39 <sup>+0.08</sup> <sub>-0.07</sub>	0.850±0.003	3.1 <sup>+0.4</sup> <sub>-0.3</sub>	-	-
1.51	0.340±0.005	(1.0)	0.680±0.008	0.45±0.01	0.850±0.003	2.9±0.3	-	-
1.58	0.340±0.006	(1.0)	0.680±0.006	0.62±0.08	0.850 <sup>+0.003</sup> <sub>-0.004</sub>	3.3 <sup>+0.5</sup> <sub>-0.4</sub>	-	-
1.64	0.340±0.006	(1.0)	0.670±0.005	0.84 <sup>+0.10</sup> <sub>-0.09</sub>	0.840 <sup>+0.004</sup> <sub>-0.005</sub>	3.4 <sup>+0.8</sup> <sub>-0.5</sub>	-	-
1.71	0.340±0.006	(1.0)	0.670±0.004	1.10 <sup>+0.08</sup> <sub>-0.07</sub>	0.840±0.003	3.4 <sup>+0.6</sup> <sub>-0.4</sub>	-	-
2.03	0.300 <sup>+0.013</sup> <sub>-0.030</sub>	(1.0)	0.670±0.003	1.80 <sup>+0.12</sup> <sub>-0.12</sub>	-	-	-	-
2.16	0.320 <sup>+0.007</sup> <sub>-0.009</sub>	(1.0)	0.660±0.002	2.50±0.11	-	-	-	-
2.29	0.310 <sup>+0.009</sup> <sub>-0.012</sub>	(1.0)	0.660±0.003	2.60 <sup>+0.16</sup> <sub>-0.15</sub>	-	-	-	-
2.42	0.320 <sup>+0.008</sup> <sub>-0.009</sub>	(1.0)	0.660±0.002	2.90 <sup>+0.18</sup> <sub>-0.16</sub>	-	-	-	-
3.06	(0.300)	(1.0)	0.650±0.004	2.60±0.20	-	-	-	-
3.13	(0.300)	(1.0)	0.660±0.003	2.90±0.20	-	-	-	-
4.29	(0.300)	(1.0)	-	-	-	-	-	-

- Darnley, M. J., Henze, M., Bode, M. F., et al. 2016, *ApJ*, 833, 149
- Dickey, J. M., & Lockman, F. J. 1990, *ARA&A*, 28, 215
- Drake, J. J., Ness, J.-U., Page, K. L., et al. 2021, *ApJL*, 922, L42
- Evans, I. N., Primini, F. A., Glotfelty, K. J., et al. 2010, *ApJS*, 189, 37
- Fruscione, A., McDowell, J. C., Allen, G. E., et al. 2006, in *Society of Photo-Optical Instrumentation Engineers (SPIE) Conference Series*, Vol. 6270, *Observatory Operations: Strategies, Processes, and Systems*, ed. D. R. Silva & R. E. Doxsey, 62701V
- Gabriel, C., Denby, M., Fyfe, D. J., et al. 2004, in *Astronomical Data Analysis Software and Systems (ADASS) XIII*, Vol. 314, *The XMM-Newton SAS - Distributed Development and Maintenance of a Large Science Analysis System: A Critical Analysis*, ed. F. Ochsenbein, M. G. Allen, & D. Egret (San Francisco, CA: ASP), 759
- Gaudin, T. M., Coe, M. J., Kennea, J. A., et al. 2024, arXiv e-prints, arXiv:2408.01388
- Gies, D. R., Wang, L., & Klement, R. 2023, *ApJL*, 942, L6
- Götberg, Y., de Mink, S. E., Groh, J. H., et al. 2018, *A&A*, 615, A78
- Graczyk, D., Pietrzyński, G., Thompson, I. B., et al. 2020, *ApJ*, 904, 13
- Greiner, J., Hasinger, G., & Kahabka, P. 1991, *A&A*, 246, L17
- Haberl, F., Maitra, C., Greiner, J., et al. 2020, *The Astronomer's Telegram*, 13789, 1
- Habets, G. M. H. J. 1986a, *A&A*, 167, 61
- . 1986b, *A&A*, 165, 95
- Hachisu, I., Kato, M., Kiyota, S., et al. 2006, *ApJL*, 651, L141
- Henze, M., Pietsch, W., Haberl, F., et al. 2010, *A&A*, 523, A89
- Hunter, J. D. 2007, *Computing in Science and Engineering*, 9, 90
- Israel, G. L., & Stella, L. 1996, *ApJ*, 468, 369
- Jaisawal, G. K., Guillot, S., Ng, M., et al. 2024, *The Astronomer's Telegram*, 16636, 1
- Kahabka, P., Haberl, F., Payne, J. L., & Filipović, M. D. 2006, *A&A*, 458, 285
- Kennea, J. A., Coe, M. J., Evans, P. A., et al. 2021, *MNRAS*, 508, 781
- Kennea, J. A., Coe, M. J., Evans, P. A., Waters, J., & Jasko, R. E. 2018, *ApJ*, 868, 47
- Kennea, J. A., Coe, M. J., Gaudin, T., & Evans, P. A. 2024, *The Astronomer's Telegram*, 16633, 1

- Li, K. L., Kong, A. K. H., Charles, P. A., et al. 2012, *ApJ*, 761, 99
- Maravelias, G., Zezas, A., Antoniou, V., & Hatzidimitriou, D. 2014, *MNRAS*, 438, 2005
- Marino, A., Russell, T. D., Del Santo, M., et al. 2023, *MNRAS*, 525, 2366
- Morii, M., Tomida, H., Kimura, M., et al. 2013, *ApJ*, 779, 118
- Nasa High Energy Astrophysics Science Archive Research Center (Heasarc). 2014, HEASoft: Unified Release of FTOOLS and XANADU, Astrophysics Source Code Library, record ascl:1408.004, ,
- Ness, J. U., Osborne, J. P., Henze, M., et al. 2013, *A&A*, 559, A50
- Orio, M., Gendreau, K., Giese, M., et al. 2022, *ApJ*, 932, 45
- . 2023, *ApJ*, 955, 37
- Osborne, J. P., Page, K. L., Beardmore, A. P., et al. 2011, *ApJ*, 727, 124
- Page, K. L., Osborne, J. P., Kuin, N. P. M., et al. 2015, *MNRAS*, 454, 3108
- Page, K. L., Kuin, N. P. M., Beardmore, A. P., et al. 2020, *MNRAS*, 499, 4814
- Raguzova, N. V. 2001, *A&A*, 367, 848
- Ransom, S. M., Eikenberry, S. S., & Middleditch, J. 2002, *AJ*, 124, 1788
- Rauch, T. 2003, *A&A*, 403, 709
- Sarraj, I., Sanders, R. J., & Schmidtke, P. C. 2012, *Information Bulletin on Variable Stars*, 6030, 1
- Schaller, G., Schaerer, D., Meynet, G., & Maeder, A. 1992, *A&AS*, 96, 269
- Sheets, H. A., Bolatto, A. D., van Loon, J. T., et al. 2013, *ApJ*, 771, 111
- Soraisam, M. D., Gilfanov, M., Wolf, W. M., & Bildsten, L. 2016, *MNRAS*, 455, 668
- Sturm, R., Haberl, F., Pietsch, W., et al. 2012, *A&A*, 537, A76
- Suleimanov, V. F., Tavleev, A. S., Doroshenko, V., & Werner, K. 2024, *A&A*, 688, A39
- Taguchi, K., Maeda, K., Maehara, H., et al. 2023, *ApJ*, 958, 156
- Tauris, T. M., & van den Heuvel, E. P. J. 2023, *Physics of Binary Star Evolution. From Stars to X-ray Binaries and Gravitational Wave Sources*. Princeton University Press., doi:10.48550/arXiv.2305.09388
- Treiber, H., Haberl, F., Vasilopoulos, G., Bailyn, C. D., & Udalski, A. 2024, *The Astronomer's Telegram*, 16638, 1
- Verner, D. A., Ferland, G. J., Korista, K. T., & Yakovlev, D. G. 1996, *ApJ*, 465, 487
- Wilms, J., Allen, A., & McCray, R. 2000, *ApJ*, 542, 914
- Wolf, W. M., Bildsten, L., Brooks, J., & Paxton, B. 2013, *ApJ*, 777, 136
- Woosley, S. E. 2019, *ApJ*, 878, 49
- Yang, H. N., Chen, W., Pan, X., et al. 2024, *The Astronomer's Telegram*, 16631, 1
- Yuan, W., Zhang, C., Chen, Y., & Ling, Z. 2022, in *Handbook of X-ray and Gamma-ray Astrophysics*, 86
- Zhu, C.-H., Lü, G.-L., Lu, X.-Z., & He, J. 2023, *Research in Astronomy and Astrophysics*, 23, 025021